© 2019. Published by The Company of Biologists Ltd | Journal of Experimental Biology (2019) 222, jeb209783. doi:10.1242/jeb.209783

SHORT COMMUNICATION

XROMM kinematics of ventilation in wild turkeys (*Meleagris gallopavo*)

Robert J. Brocklehurst[1,*,‡], Sabine Moritz[2,3], Jonathan Codd[4], William I. Sellers[1] and Elizabeth L. Brainerd[2]

ABSTRACT

The avian ribcage is derived relative to other amniotes, and is hypothesised to be constrained in its movements during ventilation. The double-headed ribs form two articulations with the vertebrae, and are thought to rotate about a strict anatomical axis. However, this costovertebral joint constraint has not been demonstrated empirically and was not found in other taxa with double-headed ribs (i.e. crocodilians). Here, we used X-ray reconstruction of moving morphology (XROMM) to quantify rib rotation in wild turkeys (*Meleagris gallopavo*) during breathing. We demonstrate that, as predicted from anatomy, the ribs do rotate in a hinge-like manner about a single axis. There is also evidence for elliptical motion of the sternum, as has been reported in other taxa. The evolution of the avian ribcage is closely related to the co-evolution of ventilation and flight, and these results are important for how we model ventilation mechanics in living and fossil birds.

KEY WORDS: Aves, Breathing, X-ray reconstruction of moving morphology, Sternum, Vertebral rib

INTRODUCTION

Birds are the most numerous group of extant tetrapods, with over 10,000 living species (Jetz et al., 2012), and understanding the factors that led to their evolutionary diversification is a key question in evolutionary biology. The avian respiratory system is highly derived and efficient compared with other amniotes (Maina, 2006). The immobile, highly subdivided parabronchial lungs are ventilated by a system of compliant air sacs (Duncker, 1972; Maina, 2006). Airflow through the lungs is unidirectional and is controlled via a system of aerodynamic valves and pressure differences between the cranial and caudal air sacs (Kuethe, 1988; Wang et al., 1988; Maina et al., 2009). However, the skeletal kinematics of ventilation that drive changes in air sac pressure and so underpin the avian respiratory system remain relatively unexplored (but see Claessens, 2004, 2009). In order to understand respiratory evolution in birds, it is important to understand the form–function relationships between ribcage morphology and the mechanics of ventilation.

The avian thorax is also derived relative to other amniotes (Baumel, 1993; Claessens, 2009; Schachner et al., 2009). The dorsal series is very short, and the ribs are bipartite, consisting of ossified vertebral and sternal segments (Fig. 1A). The sternum is also ossified, and expanded posteriorly. The vertebral ribs articulate with the vertebral column at the costovertebral joints (Fig. 1B), which are bicondylar with two distinct articulations between the rib heads and the dorsal vertebrae; the rib capitulum with the parapophysis on the vertebral centrum, and the rib tuberculum with the vertebral diapophysis at the end of the transverse process (Fig. 1B).

The bicondylar articulation at the costovertebral joint in birds is thought to move in a hinge-like manner (Claessens, 2009), with the ribs rotating about a constrained axis of rotation that passes through the diapophysis and parapophysis. However, this hypothesis has not been tested experimentally; previous studies used two-dimensional single-plane fluoroscopy (Claessens, 2009), which cannot capture details of non-planar motion, and so cannot fully describe the complex, three-dimensional motion of the ribs during ventilation (Brainerd, 2015). As for the sternum, an elliptical motion path has been documented in some birds (Claessens, 2009), but it is unclear how widespread this is. Differences in kinematic timing of the vertebral and sternal ribs have been suggested to cause elliptical motion of the sternum, but this has also not been definitively shown (Claessens, 2009).

Here, we analysed the skeletal kinematics of ventilation in wild turkeys (*Meleagris gallopavo* Linnaeus 1758) using marker-based X-ray reconstruction of moving morphology (XROMM). XROMM allows us to capture all possible translations and rotations that may occur across joints during their motion, and permits truly three-dimensional motion analysis (i.e. six degree-of-freedom motion analysis) in a morphological context (Brainerd et al., 2010). Using these XROMM data, we tested whether the ribs in *M. gallopavo* really do follow a hinge-like pattern of rotation, as predicted from the anatomy of the costovertebral joint. The motion of the sternum was also analysed in detail to determine whether there is evidence for an elliptical motion path during ventilation.

MATERIALS AND METHODS

XROMM data collection

Data were collected from three adult wild turkeys with a body mass range of 4.75–6.3 kg. Birds were captive bred and obtained from a heritage breeder. All animal care and experimental procedures were approved by the Institutional Animal Care and Use Committee of Brown University. The birds were anaesthetised, and radio-opaque markers were implanted to track the motions of the vertebrae, ribs and sternum. Tantalum beads (1 mm) were implanted into the sternal keel and all other bones were marked using conical carbide markers, ∼2.5 mm long and 0.8 mm diameter at the widest point (Kambic et al., 2014). The vertebral column and sternum were marked in all individuals; however, not all ribs could be marked in each bird, and so to ensure the whole ribcage was covered, different ribs were marked in different birds.

X-ray video data were collected at the W. M. Keck Foundation XROMM Facility, Brown University, using a custom biplanar

[1]School of Earth and Environmental Sciences, University of Manchester, Manchester M13 9PT, UK. [2]Department of Ecology and Evolutionary Biology, Brown University, Providence, RI 02912, USA. [3]Department of Biology, Community College of Rhode Island, Warwick, RI 02886, USA. [4]Faculty of Biology, Medicine and Health, University of Manchester, Manchester M13 9PT, UK.
‡Present address: Museum of Comparative Zoology and Department of Organismic and Evolutionary Biology, Harvard University, Cambridge, MA 02138, USA.

*Author for correspondence (rbrocklehurst@fas.harvard.edu)

R.J.B., 0000-0002-3017-6838; J.C., 0000-0003-0211-1786; W.I.S., 0000-0002-2913-5406; E.L.B., 0000-0003-0375-8231

Received 30 June 2019; Accepted 30 October 2019

Journal of Experimental Biology (2019) 222, jeb209783. doi:10.1242/jeb.209783

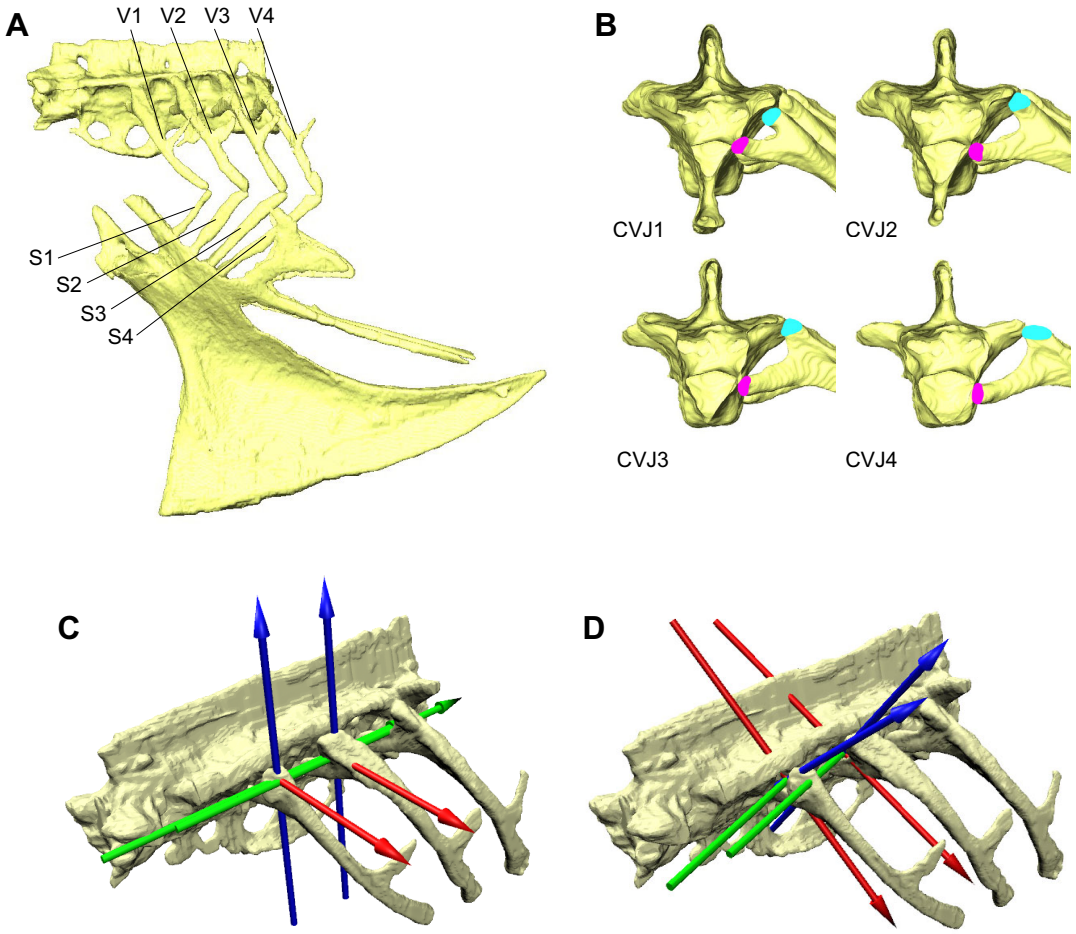

Fig. 1. Ribcage anatomy and joint coordinate systems of *Meleagris gallopavo*. (A) Left lateral view of the ribcage, with the vertebral ribs (V1–4) and sternal ribs (S1–4) labelled. (B) Frontal view of the vertebral column and proximal ribs, showing the parapophysis–capitulum (pink) and diapophysis–tuberculum (turquoise) articulations at the costovertebral joints (CVJs). (C) Costovertebral JCS (CV-JCS) axes are oriented to the primary body axes such that the dorsoventral *Z*-axis (blue) measures bucket handle motion, the craniocaudal *Y*-axis (green) measures calliper motion and the mediolateral *X*-axis (red) measures pump handle motion. (D) Parapophysis–diapophysis JCS (PD-JCS) axes oriented to pass through the parapophysis and the diapophysis such that the *Z*-axis (blue) measures flexion–extension, the *Y*-axis (green) measures abduction–adduction and the *X*-axis (red) measures long-axis rotation.

fluoroscopy setup (Miranda et al., 2011). Videos were recorded at 60 or 100 frames s^{-1}, with an exposure time of 700 µs and X-ray energy of 70–90 kV and 100–200 mA. Once video data collection was completed, the animals were euthanized and computed tomography (CT) scanned with an Animage Fidex veterinary CT scanner with isotropic voxels (0.4–0.5 mm). The raw data associated with this study (X-ray video and CT scan data) are available from the X-ray Motion Analysis Portal (xmaportal.org) and are stored in accordance with best practices for video data management in organismal biology (Brainerd et al., 2017). From the CT data, bones and markers were segmented in Avizo (Version 8.1, 9.0, FEI Visualisation Sciences Group), and 3D surface meshes were exported as OBJ files. Smoothing, cleaning and mesh reduction (retaining anatomical accuracy whilst reducing file size) were carried out in Geomagic Studio (2012, Geomagic Inc.) and Meshlab (http://meshlab.sourceforge.net/). Finally, all mesh models were imported into Autodesk Maya (Version 2016, Autodesk Inc.) for animation.

Marker positions were tracked in the X-ray videos using XMALab (Knörlein et al., 2016) to a precision of ±0.12 mm (calculated based on distance between intra-osseous marker pairs as in Knörlein et al., 2016). Distortion was corrected using standard grid images and the three-dimensional space was calibrated using images of a cube with 64 radio-opaque markers. All calibration files are available from the X-ray Motion Analysis Portal (xmaportal.org). Once all markers had been tracked, rigid body transformations of the vertebrae, ribs and sternum were calculated in XMALab. These transformations were then filtered with a low-pass Butterworth filter with a frequency cut-off of 5–6 Hz for the ribs and sternum, but more aggressive filtering was applied to the vertebral column (cut-off 1–2 Hz) on the grounds that it was almost stationary during ventilation. The rigid body transformations from each marker set were applied to the corresponding 3D model in Autodesk Maya to create the XROMM animations (Movie 1). Kinematic data were collected and analysed for five full breaths from one inhalation to the next for all individuals.

Joint coordinate systems

Kinematic data were extracted from the XROMM animations using local joint coordinate systems (JCSs), to measure translation and rotation across joints. One JCS was oriented relative to the body planes, in order to decompose rotations about the joints into bucket handle, pump handle and calliper motion (Brainerd et al., 2016; Brocklehurst et al., 2017). This costovertebral JCS (CV-JCS) was

positioned as follows: the *Z*-axis was oriented dorso-ventrally (dorsal is positive), representing bucket handle motion; the *Y*-axis was oriented cranio-caudally (caudal is positive), representing calliper motion; and the *X*-axis was oriented medio-laterally (left is positive), representing pump handle motion (Fig. 1C). JCSs were placed and outputs were calculated in Autodesk Maya using XROMM MayaTools (bitbucket.org/xromm/xromm_mayatools). Polarities follow the right-hand rule and Euler angles were calculated with the rotation order *ZYX*.

In addition to the JCSs described above, to test the hinge-like nature of the costovertebral joint, we used a JCS that was oriented based on the positions of the parapophysis and diapophysis – a parapophysis–diapophysis joint coordinate system (or PD-JCS) (Fig. 1D). Here, the *Z*-axis was oriented along the anatomical axis running from the parapophysis to the diapophysis, the *X*-axis ran through the rib tuberculum pointing down the vertebral rib and the *Y*-axis was orthogonal to both. In the PD-JCS, the *Z*-axis measures flexion–extension of the joint, the *Y*-axis measures abduction–adduction and the *X*-axis measures long axis rotation (Fig. 1D).

For all local coordinate systems, it was necessary to define a 'zero pose' (i.e. starting position); for this, maximum inhalation was chosen, rather than using a non-anatomical reference pose (Brocklehurst et al., 2017). It should be noted that maximum inhalation is not a resting pose in birds. To compare breaths of differing magnitude and duration, we applied a standard resampling procedure (Gidmark et al., 2014; Brocklehurst et al., 2017); data were imported into R, resampled to 100 points (each point being 1% of the breathing cycle) and zeroed to the mean angle of each rotational degree of freedom.

Precision of the rotations measured by a JCS is dependent on marker positioning within the bones, and placement of the JCS. JCS precision was measured from markers on a frozen specimen; the whole frozen specimen was manually translated and rotated in the X-ray beams, and joint rotations measured using the JCSs described above. In a frozen specimen, all joint rotations should be zero and standard deviation of the JCS output is a measure of rigid-body precision (Menegaz et al., 2015). Mean precision of rotations about the *X*-, *Y*- and *Z*-axes of the CV-JCS was 0.085, 0.250 and 0.067 deg, respectively. Mean precision of rotations about the *X*-, *Y*- and *Z*-axes of the PD-JCS was 0.101, 0.229 and 0.108 deg, respectively.

To measure the motion path of the sternum, a reference 'body' coordinate system was positioned and oriented based on the vertebral column. In this system, the *Z*-axis pointed dorsally, the *Y*-axis pointed caudally and the *X*-axis pointed to the left. The translation and position of the posterior tip of the sternal keel was then measured in this reference coordinate system. To test for differences in kinematic timing that might create elliptical sternal motion, we also measured the translation of the distal tip of the vertebral and sternal ribs, using the same reference coordinate system as for the sternum. These data were imported into R, the peaks and valleys corresponding to maximum expiration and inspiration were located, and their positions were compared to check for consistent differences in kinematic timing.

RESULTS & DISCUSSION

The costovertebral joint

From the XROMM animations, we have two different ways of measuring the 3D motions occurring at the costovertebral joint: the standard CV-JCSs oriented to the body axes, and the PD-JCSs oriented to the parapophysis and diapophysis. From the CV-JCS data, bucket and pump handle motions occur in roughly equal measure, and account for the majority of the rotations occurring at the costovertebral joint in all ribs (Fig. 2A,B). This matches our predictions based on joint morphology. There is some calliper motion measured using the CV-JCSs, but this has a relatively minor contribution to motion across the joint. Although pump and bucket handle motion are mostly in phase, a slight phase difference can be seen in some plots (e.g. costovertebral joint 2 and 4 of Me23 and Me49, respectively), where pump handle motion peaks before bucket handle motion (Fig. 2A,B).

When rotations are measured using a PD-JCS, we see that the majority of the rotation occurring about the costovertebral joint can be described as flexion–extension about the anatomical *Z*-axis, running along the line between the parapophysis and diapophysis (Fig. 2C,D); this clearly shows support for a hinge-like model of rib motion in birds. There appears to be some contribution from the other two axes (representing abduction–adduction and long-axis rotation), but flexion–extension appears to dominate. Comparing the cranial and caudal parts of the ribcage, there is little variation in either the magnitude or kind of the rotations occurring at the costovertebral joint, and motions are consistent across the ribcage.

Although the motions measured in this study generally support hinge-like rotations at the costovertebral joint, the motions were never 100% hinge-like (Fig. 2D). Owing to the small magnitude of the rotations being measured in this study – generally only a few degrees at most – this is possibly a problem of signal-to-noise ratio. When we consider rigid body precision as assessed using our frozen specimen, much of the motions that occurred *in vivo* about the *X*- and *Y*-axes of the PD-JCS (Fig. 2C) actually fell within the bounds of rigid body precision (0.101 and 0.229 deg, respectively). Meanwhile, rotations about the *Z*-axis (the anatomical hinge axis) were well outside the bounds of rigid body precision (0.108 deg) (Fig. 2C), and so we can be confident that these rotations represent a genuine signal of hinge-like motion about the costovertebral joint.

These results contrast with those from the living sister taxon to birds, the crocodilians, where costovertebral anatomy was found to predict only general patterns of rib motion (Brocklehurst et al., 2017). There are several possible reasons for this difference. Birds retain the wide separation of the diapophysis and parapophysis for the whole vertebral column; in crocodilians, the parapophysis migrates towards the diapophysis, starting at the third thoracic vertebra (Schachner et al., 2009; Brocklehurst et al., 2018). The parapophyseal facets are also flatter and more medio-laterally inclined in crocodilians from the third thoracic vertebra, which may permit translation of the rib capitulum (Claessens, 2009), and allow the ribs to deviate from their anatomical hinge axis (Brocklehurst et al., 2017).

Birds also possess additional soft tissue constraints to rib motion. Two ligaments, the costotransverse ligament and the costovertebral ligament, connect the rib heads to the vertebrae in birds (Baumel, 1993; Yasuda, 2002), but are absent in crocodilians (Hirasawa, 2009). The costovertebral joint of birds is also surrounded by lung tissue, as the rib heads incise the dorsal surface of the lung (Maina and Nathaniel, 2001). This intimate association between the ribs and lung tissue would presumably restrict motion outside of rotation about an anatomical hinge axis. In crocodilians, following the migration of the parapophysis on the transverse process, the rib heads lie dorsal to the surface of the lung and so do not face those same constraints (Schachner et al., 2009; Brocklehurst et al., 2018).

Motion of the sternum

The motion path of the tip of the sternum in lateral projection appeared to be scissor-like in one individual (Me18) (Fig. 3A), but did show evidence of elliptical movement in a second (Me23) (Fig. 3B). Unfortunately, owing to issues with marker placement

Journal of Experimental Biology (2019) 222, jeb209783. doi:10.1242/jeb.209783

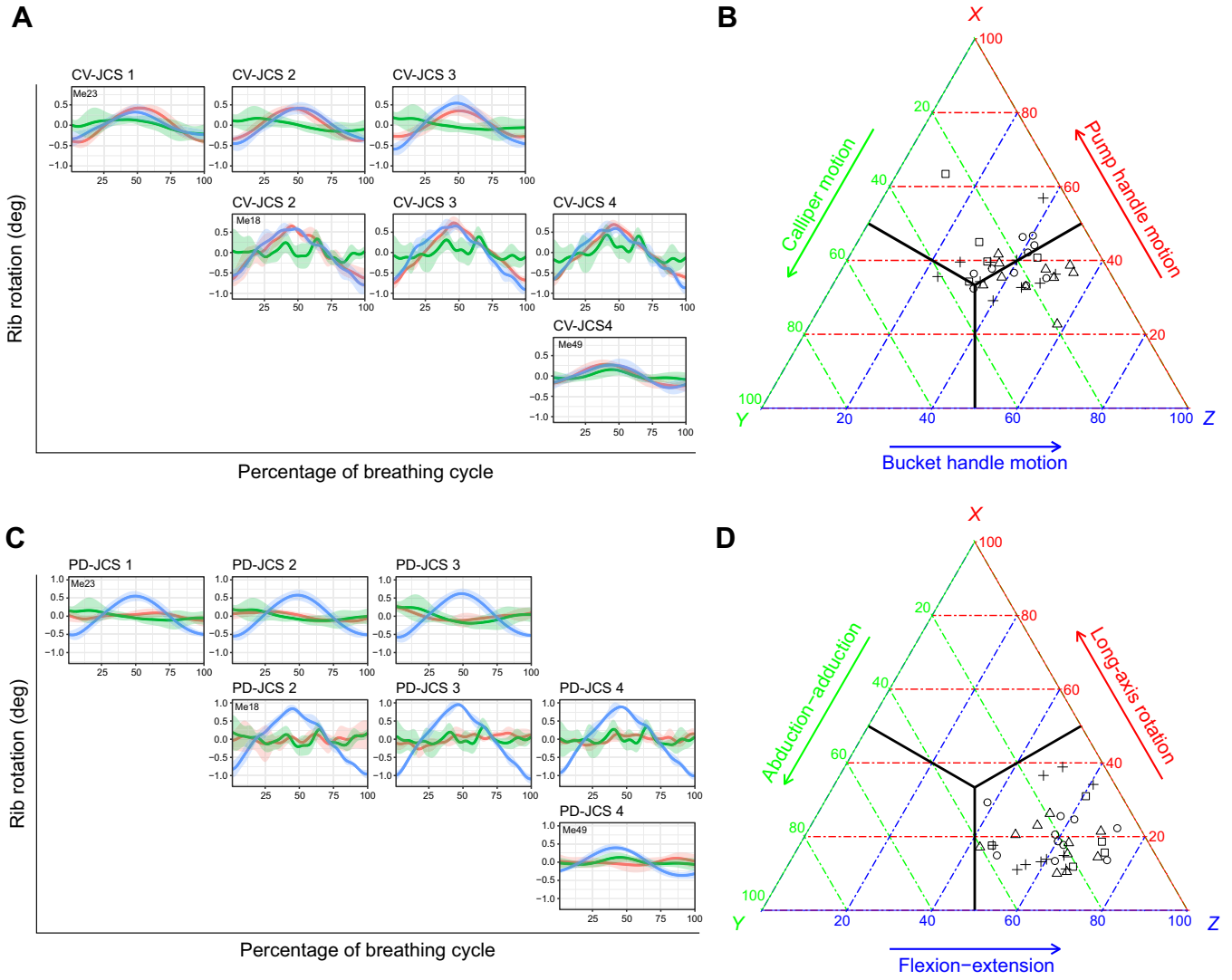

Fig. 2. Motions of the vertebral ribs in *M. gallopavo*. (A,B) Pump handle (red), calliper (green) and bucket handle (blue) motion of the vertebral rib relative to the vertebral column at the costovertebral joint, measured using a CV-JCS. (C,D) Long-axis rotation (red), abduction–adduction (green) and flexion–extension (blue) of the vertebral rib relative to the vertebral column at the costovertebral joint, measured using a PD-JCS. (A,C) Plots of each costovertebral joint from three individuals (Me23, Me18 and Me49). Graphs show means±1 s.d. (*N*=5 breaths). Breathing cycle calculated from one full inspiration to the next. (B,D) Ternary plots showing different contributions of rotations at the JCSs. Data include all joints from all individuals. Each point is one breath. Symbols represent different joints, numbered from cranial to caudal: square, CV1; circle, CV2; triangle, CV3: cross, CV4.

and tracking, it was not possible to accurately animate the sternum of our third individual (Me49). Elliptical motion of the sternum during ventilation in birds was suggested by Claessens, based on his own work and previous studies (Jenkins et al., 1988; Claessens, 2009). Scissor-like motion involves only dorsoventral rotation of the sternum, whereas elliptical motion also includes some craniocaudal translation. Although there was clear evidence for elliptical sternal movement in emu (*Dromaius novaehollandiae*), the motion appeared scissor-like or linear in other birds (Claessens, 2009). In part, this was attributed to limitations of the method (Claessens, 2009). Here, using XROMM, which has greater precision and can measure smaller motions, we found individual variation in the motion path of the sternum (Fig. 3A,B).

In Me23, which displayed elliptical sternal motion, there was some evidence for variation in kinematic timing – peak expiratory movements almost always occurred a few frames earlier in the sternal ribs, compared with the vertebral ribs (Fig. 3C,D). This pattern was also generally true of peak inspiratory movements, but was occasionally reversed (Fig. 3C,D). Elliptical motion of the sternum was hypothesised to be driven by differences in timing of the motion of the sternal ribs relative to the vertebral ribs (Claessens, 2009); if the sternum and distal sternal ribs move ventrally faster than the distal vertebral ribs move cranially during inspiration, then the sternum will be displaced both ventrally and caudally (and vice versa during expiration). Our XROMM data support this, showing some evidence for subtle differences in kinematic timing comparing craniocaudal displacement of the distal vertebral ribs with the dorsoventral displacement of the distal sternal ribs (Fig. 3C,D). Electromyographic data show the cosoternalis pars major, which inserts onto the sternal ribs (Baumel, 1993), is active earlier in inspiration than the intercostal muscles, which attach to the vertebral ribs (Fedde et al., 1964).

Elliptical motion of the sternum was thought to aid in generating and maintaining unidirectional airflow (Claessens, 2009). However, the unidirectional nature of intrapulmonary airflow is mostly governed by aerodynamic valving (Banzett et al., 1987; Wang

Journal of Experimental Biology (2019) 222, jeb209783. doi:10.1242/jeb.209783

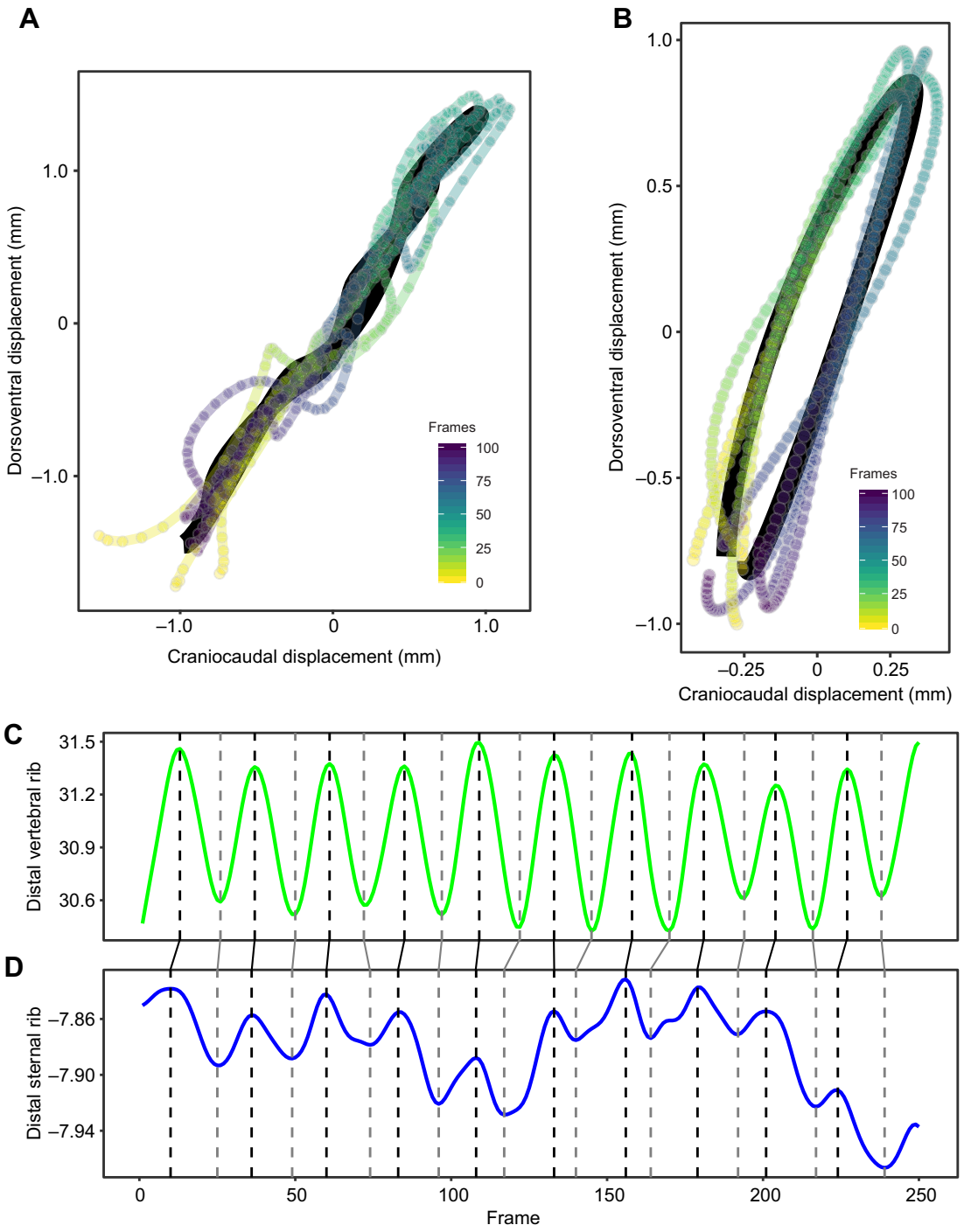

Fig. 3. Sternum motion *in vivo* during ventilation in *M. gallopavo*. (A,B) Motion path of the posterior tip of the sternum in the sagittal plane measured for five breaths in (A) Me18 (scissor-like motion) and (B) Me23 (elliptical motion). All breaths overlaid with the mean motion path shown in black. (C,D) Traces showing (C) the craniocaudal displacement (cm) of the distal verterbal rib (caudal is positive) and (D) the dorsoventral displacement (cm) of the sternal rib (dorsal is positive) of Me23, which showed elliptical sternal motion. Peaks and valleys corresponding to maximum expiratory (black) and inspiratory motions (grey), respectively, are marked by the dashed lines. Solid lines connect the same peaks between the two traces and the angle of the line indicates the degree of phase lag between the vertebral and sternal ribs.

et al., 1988; Maina et al., 2009), and experimental occlusion of the air sacs showed maintenance of aerodynamic valving and unidirectional flow (Brackenbury et al., 1989; Brackenbury and Amaku, 1990). Unidirectional flow has also been demonstrated in crocodilians (Farmer and Sanders, 2010; Schachner et al., 2013) and lepidosaurs (Schachner et al., 2014; Cieri et al., 2014), which do not ventilate their lungs via dorsoventral motion of the sternum. Therefore, elliptical sternal motion may be sufficient to help generate unidirectional flow, but is not necessary. The presence of elliptical motion seems to be related to differences in kinematic timing of the ribs (Fig. 3), and it is possible that elliptical versus scissor-like sternum motion is simply the result of variation in respiratory muscle activation patterns. Observed differences in kinematic timing were not entirely consistent (Fig. 3C,D), fitting

with the idea that elliptical sternal motion is not constrained. Our data suggest that elliptical sternal motion is a variable trait, the functional significance of which is unclear.

Concluding remarks

Along with their unique lung–air sac respiratory system, birds have also evolved a highly constrained ribcage, and a derived mode of ventilation. These two features – skeletal form and breathing function – are intimately linked, and so establishing the relationships between them is important for our understanding of the evolution of avian ventilation. The results presented here suggest that joint morphology in birds can be a good predictor of rib motion, and that sternum motion is less constrained to a particular pattern (elliptical versus scissor-like) than previously thought. This study serves both to demonstrate the strength of XROMM, measuring detailed three-dimensional skeletal kinematics in the context of bone and joint morphology, and as an empirical framework in which modelling studies may have their assumptions based and their outputs validated. The results presented here deepen our understanding of the relationship between ventilation and trunk skeletal morphology, and open the possibility for future work on how these features vary with ecology in modern birds, and how they evolved through time across the dinosaur–bird transition.

Acknowledgements

We thank J. D. Laurence-Chasen, K. K. Stover and E. G. Tavares for assistance with animal husbandry, surgeries and data collection, and C. Walmsley for assistance with data analysis. We thank D. B. Baier and S. M. Gatesy for XROMM MayaTools. We thank E. Kaczmarek for assisting with the precision study.

Competing interests

The authors declare no competing or financial interests.

Author contributions

Conceptualization: S.M., E.L.B.; Methodology: S.M., E.B.; Formal analysis: R.J.B., S.M., E.B.; Investigation: R.J.B., S.M., E.L.B.; Resources: W.S., E.B.; Writing - original draft: R.J.B.; Writing - review & editing: R.J.B., J.C., W.S., E.L.B.; Visualization: R.J.B.; Supervision: J.C., W.S., E.B.; Funding acquisition: J.C., W.S., E.B.

Funding

This work was supported by the US National Science Foundation [1120967 and 1661129]. R.J.B. was supported by a studentship at the University of Manchester as part of a UK Biotechnology and Biological Sciences Research Council Doctoral Training Partnership [BB/M011208/1].

Data availability

Data have been deposited in the XMAPortal (xmaportal.org) in the study 'Turkey Lung Ventilation' with permanent ID BROWN45.

Supplementary information

Supplementary information available online at
http://jeb.biologists.org/lookup/doi/10.1242/jeb.209783.supplemental

References

Banzett, R. B., Butler, J. P., Nations, C. S., Barnas, G. M., Lehr, J. L. and Jones, J. H. (1987). Inspiratory aerodynamic valving in goose lungs depends on gas density and velocity. *Respir. Physiol.* **70**, 287-300. doi:10.1016/S0034-5687(87)80051-8

Baumel, J. J. ed. (1993). *Handbook of avian anatomy: nomina anatomica avium*. 2nd edn. Cambridge, MA: Nuttall Ornithological Club.

Brackenbury, J. and Amaku, J. (1990). Effects of combined abdominal and thoracic air-sac occlusion on respiration in domestic fowl. *J. Exp. Biol.* **152**, 93-100.

Brackenbury, J. H., Darby, C. and El-Sayed, M. S. (1989). Respiratory function in exercising fowl following occlusion of the thoracic air sacs. *J. Exp. Biol.* **145**, 227-237.

Brainerd, E. L. (2015). Major transformations in vertebrate breathing mechanisms. In *Great Transformations in Vertebrate Evolution* (ed. K. P. Dial, N. H. Shubin and E. L. Brainerd), pp. 47-62. Chicago University Press.

Brainerd, E. L., Baier, D. B., Gatesy, S. M., Hedrick, T. L., Metzger, K. A., Gilbert, S. L. and Crisco, J. J. (2010). X-ray reconstruction of moving morphology (XROMM): precision, accuracy and applications in comparative biomechanics research. *J. Exp. Zool. Part Ecol. Genet. Physiol.* **313A**, 262-279. doi:10.1002/jez.589

Brainerd, E. L., Moritz, S. and Ritter, D. A. (2016). XROMM analysis of rib kinematics during lung ventilation in the green iguana, Iguana iguana. *J. Exp. Biol.* **219**, 404-411. doi:10.1242/jeb.127928

Brainerd, E. L., Blob, R. W., Hedrick, T. L., Creamer, A. T. and Müller, U. K. (2017). Data management rubric for video data in organismal biology. *Integr. Comp. Biol.* **57**, 33-47. doi:10.1093/icb/icx060

Brocklehurst, R. J., Moritz, S., Codd, J., Sellers, W. I. and Brainerd, E. L. (2017). Rib kinematics during lung ventilation in the American alligator (*Alligator mississippiensis*): an XROMM analysis. *J. Exp. Biol.* **220**, 3181-3190. doi:10.1242/jeb.156166

Brocklehurst, R. J., Schachner, E. R. and Sellers, W. I. (2018). Vertebral morphometrics and lung structure in non-avian dinosaurs. *Open Sci.* **5**, 180983. doi:10.1098/rsos.180983

Cieri, R. L., Craven, B. A., Schachner, E. R. and Farmer, C. G. (2014). New insight into the evolution of the vertebrate respiratory system and the discovery of unidirectional airflow in iguana lungs. *Proc. Natl. Acad. Sci. USA* **111**, 17218-17223. doi:10.1073/pnas.1405088111

Claessens, L. P. A. M. (2004). Archosaurian respiration and the pelvic girdle aspiration breathing of crocodyliforms. *Proc. R. Soc. Lond. B Biol. Sci.* **271**, 1461-1465. doi:10.1098/rspb.2004.2743

Claessens, L. P. A. M. (2009). The skeletal kinematics of lung ventilation in three basal bird taxa (emu, tinamou, and guinea fowl). *J. Exp. Zool. Part Ecol. Genet. Physiol.* **311A**, 586-599. doi:10.1002/jez.501

Duncker, H.-R. (1972). Structure of avian lungs. *Respir. Physiol.* **14**, 44-63. doi:10.1016/0034-5687(72)90016-3

Farmer, C. G. and Sanders, K. (2010). Unidirectional airflow in the lungs of alligators. *Science* **327**, 338-340. doi:10.1126/science.1180219

Fedde, M. R., Burger, R. E. and Kitchell, R. L. (1964). Electromyographic studies of the effects of bodily position and anesthesia on the activity of the respiratory muscles of the domestic cock. *Poult. Sci.* **43**, 839-846. doi:10.3382/ps.0430839

Gidmark, N. J., Tarrant, J. C. and Brainerd, E. L. (2014). Convergence in morphology and masticatory function between the pharyngeal jaws of grass carp, *Ctenopharyngodon idella*, and oral jaws of amniote herbivores. *J. Exp. Biol.* **217**, 1925-1932. doi:10.1242/jeb.096248

Hirasawa, T. (2009). The ligamental scar in the costovertebral articulation of the tyrannosaurid dinosaurs. *Acta Palaeontol. Pol.* **54**, 49-59. doi:10.4202/app.2009.0106

Jenkins, F. A., Dial, K. P. and Goslow, G. E. (1988). A cineradiographic analysis of bird flight: the wishbone in starlings is a spring. *Science* **241**, 1495-1498. doi:10.1126/science.241.4872.1495

Jetz, W., Thomas, G. H., Joy, J. B., Hartmann, K. and Mooers, A. O. (2012). The global diversity of birds in space and time. *Nature* **491**, 444. doi:10.1038/nature11631

Kambic, R. E., Roberts, T. J. and Gatesy, S. M. (2014). Long-axis rotation: a missing degree of freedom in avian bipedal locomotion. *J. Exp. Biol.* **217**, 2770-2782. doi:10.1242/jeb.101428

Knörlein, B. J., Baier, D. B., Gatesy, S. M., Laurence-Chasen, J. D. and Brainerd, E. L. (2016). Validation of XMALab software for marker-based XROMM. *J. Exp. Biol.* **219**, 3701-3711. doi:10.1242/jeb.145383

Kuethe, D. O. (1988). Fluid mechanical valving of air flow in bird lungs. *J. Exp. Biol.* **136**, 1-12.

Maina, J. N. (2006). Development, structure, and function of a novel respiratory organ, the lung-air sac system of birds: to go where no other vertebrate has gone. *Biol. Rev.* **81**, 545-579. doi:10.1017/S1464793106007111

Maina, J. N. and Nathaniel, C. (2001). A qualitative and quantitative study of the lung of an ostrich, *Struthio camelus*. *J. Exp. Biol.* **204**, 2313-2330.

Maina, J. N., Singh, P. and Moss, E. A. (2009). Inspiratory aerodynamic valving occurs in the ostrich, *Struthio camelus* lung: a computational fluid dynamics study under resting unsteady state inhalation. *Respir. Physiol. Neurobiol.* **169**, 262-270. doi:10.1016/j.resp.2009.09.011

Menegaz, R. A., Baier, D. B., Metzger, K. A., Herring, S. W. and Brainerd, E. L. (2015). XROMM analysis of tooth occlusion and temporomandibular joint kinematics during feeding in juvenile miniature pigs. *J. Exp. Biol.* **218**, 2573-2584. doi:10.1242/jeb.119438

Miranda, D. L., Schwartz, J. B., Loomis, A. C., Brainerd, E. L., Fleming, B. C. and Crisco, J. J. (2011). Static and dynamic error of a biplanar videoradiography system using marker-based and markerless tracking techniques. *J. Biomech. Eng.* **133**, 121002. doi:10.1115/1.4005471

Schachner, E. R., Lyson, T. R. and Dodson, P. (2009). Evolution of the respiratory system in nonavian theropods: evidence from rib and vertebral morphology. *Anat. Rec. Adv. Integr. Anat. Evol. Biol.* **292**, 1501-1513. doi:10.1002/ar.20989

Schachner, E. R., Hutchinson, J. R. and Farmer, C. G. (2013). Pulmonary anatomy in the Nile crocodile and the evolution of unidirectional airflow in Archosauria. *PeerJ* **1**, e60. doi:10.7717/peerj.60

Schachner, E. R., Cieri, R. L., Butler, J. P. and Farmer, C. G. (2014). Unidirectional pulmonary airflow patterns in the savannah monitor lizard. *Nature* **506**, 367-370. doi:10.1038/nature12871

Wang, N., Banzett, R. B., Butler, J. P. and Fredberg, J. J. (1988). Bird lung models show that convective inertia effects inspiratory aerodynamic valving. *Respir. Physiol.* **73**, 111-124. doi:10.1016/0034-5687(88)90131-4

Yasuda, M. (2002). *The Anatomical Atlas of Gallus*. University of Tokyo Press.

Movie 1. XROMM animation of the ribcage of a wild turkey (*Melagris gallopavo*) during ventilation. Playback is at quarter speed.